

Laser polarimetric measurement of equilibrium and fluctuating magnetic fields in a reversed field pinch (invited)

D. L. Brower,^{a)} W. X. Ding, and S. D. Terry

Electrical Engineering Department, University of California at Los Angeles, Los Angeles, California 90095

J. K. Anderson, T. M. Biewer, B. E. Chapman, D. Craig, C. B. Forest, S. C. Prager,
and J. S. Sarff

Physics Department, University of Wisconsin-Madison, Madison, Wisconsin 53706

(Presented on 8 July 2002)

New developments in Faraday rotation polarimetry have provided the first measurements of current density profile and core magnetic fluctuations in the core of a high-temperature reversed field pinch. This has been achieved by a fast-polarimeter system with time response up to 1 μ s and phase resolution <1 mrad. Recent experiments on Madison Symmetric Torus have directly measured radial magnetic field fluctuations in the plasma interior with amplitude 33 G, $\sim 1\%$. A broad spectrum of magnetic fluctuations is observed up to 100 kHz. Relaxation of the current density profile at the sawtooth crash occurs on the timescale of 100 μ s. Reversed-field pinch behavior is determined in large part by magnetic fluctuations driven by the radial gradient in the parallel current density. Hence, measurement of magnetic fluctuations and the current density profile is essential to understand the link between the current density profile, fluctuations, and transport. © 2003 American Institute of Physics. [DOI: 10.1063/1.1526927]

I. INTRODUCTION

Understanding plasma stability and confinement in a reversed-field pinch (RFP), or any toroidal confinement device, requires detailed information on the internal magnetic field structure and current density distribution. The stability of the plasma to tearing modes and other magnetohydrodynamics (MHD) events such as the sawtooth perturbation or dynamo are closely related to the current density profile. In RFPs, resistive MHD instabilities can produce magnetic islands on rational surfaces that are closely spaced in radius causing magnetic stochasticity resulting from island overlap. Energy transport in conventional RFP plasmas is believed to arise mainly from particles streaming along these stochastic magnetic field lines. For the Madison Symmetric Torus (MST), a major goal is to reduce magnetic fluctuations through current density profile control. Elucidating the physics of this interplay requires high-resolution measurement of both the current density profile time evolution and magnetic fluctuations.

Motivated by the need to address these critical measurement needs within the RFP community and the potential application to other toroidal confinement devices (such as the tokamak), a new high-resolution polarimeter-interferometer system (POLARIS) is being developed to measure the plasma poloidal magnetic field profile and magnetic fluctuations, as well as the electron density profile and density fluctuations in the core of a high-temperature plasma. The diagnostic being developed will provide a nonperturbing measure of the spatial distribution of both the equilibrium and fluctuating quantities. Time resolution of the simultaneous polarimeter-interferometer system will be ~ 4 μ s. This reso-

lution will be sufficient to measure perturbed equilibrium profiles on the time scale of the sawtooth crash and high-frequency small-amplitude magnetic fluctuations. The fast time resolution and small-amplitude phase resolution have already been demonstrated by the interferometer.^{1,2}

To date, the maximum bandwidth achieved by polarimetry-interferometry systems in plasma applications has been 5 kHz using amplitude techniques³ and 1 kHz by phase measurement techniques.⁴ This is insufficient to see fast changes to the equilibrium profiles or the magnetic fluctuations of interest in the MST. Observations made by external magnetic probes show fluctuations at frequencies up to and well beyond 100 kHz which are dominated by resistive tearing modes in the range of 5–30 kHz with fractional amplitudes $\bar{B}/B_0 \approx 1\%$. In order to observe these frequencies, a polarimeter-interferometer system is currently being developed and tested which will employ a three-wave far-infrared laser. This approach, originally proposed by Dodel and Kunz,⁵ produces a phase measurement and involves the launching of two waves into the plasma that are circularly polarized and counter rotating. Previous phase measurement techniques involved mechanically spinning wave plates which generated a rotating, linearly polarized beam.⁶ In such systems, the bandwidth is limited by the plate rotation speed and phase noise generated by the mechanical rotator limited the phase resolution.

The Dodel and Kunz technique has been previously used to obtain information on equilibrium profiles. Single and multichannel systems have been developed and employed (with varying degrees of success) on the ZT-40M reversed-field pinch,⁷ RTP tokamak,^{8,9} LHD stellarator,¹⁰ and a field reversed configuration.¹¹ However, the potential for high time response has never before been exploited to investigate

^{a)}Electronic mail: brower@mail.utexas.edu

fast changes to equilibrium profiles or broadband magnetic fluctuations. Fast time response with high phase resolution will be the focus of the new work presented in this article.

Laser polarimetry has been used previously to investigate magnetic fluctuations associated with the coherent $m = 1, n = 1$ MHD modes (~ 2 kHz) on the TEXTOR tokamak.¹² This single-chord system had maximum time response of 0.2 ms. Other approaches used to measure the interior magnetic field structure and fluctuations in high-temperature plasmas include a heavy ion beam probe on the TEXT tokamak which measured core magnetic perturbations associated with a $m = 2, n = 1$ MHD mode (~ 3 kHz).¹³ In addition, cross polarization scattering was used on the TORE Supra tokamak to study short wavelength ($k \sim 12 \text{ cm}^{-1}$) magnetic fluctuations.¹⁴ We extend these efforts to include measurement of the broadband magnetic fluctuation amplitude, frequency and wave number spectrum, and behavior changes in improved confinement plasmas.

The remainder of the article is organized as follows: First, the diagnostic approach and system will be described. Modifications necessary to realize the fast time response will be highlighted. Second, experimental results from the MST RFP will be presented for both (1) fast changes to the equilibrium profile and (2) core measurement of magnetic fluctuations. Finally, we will conclude by pointing out future directions of diagnostic development and their application to fusion plasma research.

II. POLARIMETER-INTERFEROMETER SYSTEM

The fast-polarimetry technique employed on MST utilizes two distinct but collinear far-infrared (FIR) laser beams to probe the plasma. A third FIR laser, serving as the local-oscillator (LO) drive for the mixers, can be added to provide a simultaneous polarimetry-interferometry capability to measure both the plasma density and Faraday rotation.^{8,9} The method basically involves two separate phase measurements using orthogonally polarized waves, the polarization of each remaining stationary. The interferometric phase and Faraday angle are obtained by combining these two measurements. Since no mechanical polarization modulation is used, modulation artifacts which contaminate the phase are also absent. The achievable temporal resolution is, in principle, limited by the frequency offset of the laser beams and can be set to $< 1 \mu\text{s}$. The technique employed has been previously described and will only be briefly reviewed here.^{5,8,9}

A schematic the three-laser setup is shown in Fig. 1. The two probing beams are slightly frequency offset and their polarizations are set to counter-rotating circular. This is achieved by making the two linearly polarized beams orthogonal via use of a $\lambda/2$ wave plate and combining them through use of a polarizing beamsplitter to be collinear. The collinear beams are then passed through a $\lambda/4$ wave plate generating the counter-rotating circularly polarized beams. Upon emerging from the plasma, the probing beams pass through a polarizer that transmits the polarization component in the toroidal direction. The two probe beams, which were initially orthogonal, are then combined with the linearly polarized local-oscillator beam, which is also frequency offset

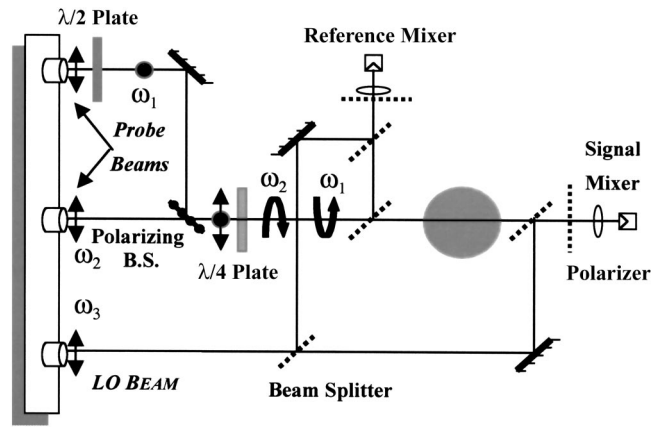


FIG. 1. Schematic of MST three-wave FIR polarimeter-interferometer system.

from the two probe beams, to give a total of three primary intermediate-frequency (IF) signals multiplexed at the detector. A portion of each beam is collected before reaching the plasma and used to generate a reference waveform for each of the mixing products. The phase difference between reference and plasma signals is then evaluated at each IF frequency.

Because of plasma birefringence, each beam experiences a different value of refractive index while propagating through the plasma. The difference in refractive index for the right (n_R)- and left (n_L)-hand circularly polarized waves is related to the Faraday rotation angle, Ψ , by the relation:

$$\Psi = \frac{2\pi}{\lambda} \int \frac{(n_R - n_L)}{2} dz = 2.62 \times 10^{-13} \lambda^2 \int n_e(z) B_{\parallel}(z) dz, \quad (1)$$

where B_{\parallel} is the component of the magnetic field parallel to the FIR beam, n_e is the electron density, and λ is the FIR laser wavelength, all in MKS units. Since n_e is known from the interferometer measurement, the poloidal magnetic field can be determined from inversion of the above equation. The toroidal current density is then obtained from Ampere's law. The average refractive index is related to the density phase shift according to

$$\Phi = \frac{2\pi}{\lambda} \int \frac{(n_R + n_L)}{2} dz \approx 2.82 \times 10^{-15} \lambda \int n_e(z) dz. \quad (2)$$

The frequency offsets that allow us to isolate and separately demodulate the independent carriers are generated by proper tuning of the three FIR laser cavities. Phase information is recovered from each of the three independent mixing products. First, mixing between the right- (left) circularly polarized probe beam and the LO gives phase information on the refractive index for the R -(L -) wave. Second, mixing of the two signal beams provides phase information that is directly proportional to the Faraday rotation angle. This quantity can also be obtained indirectly by taking the difference between the phases of the probe-LO mixing products [see Eq. (1)]. The interferometer phase shift is obtained by taking the av-

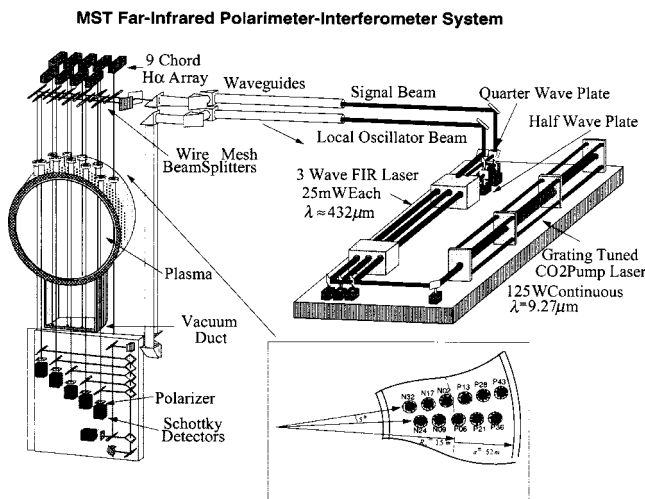


FIG. 2. Three-wave FIR polarimeter–interferometer system proposed for MST.

erage of the two probe-LO phases [see Eq. (2)]. Since the FIR source frequency (694 GHz) is much greater than the electron cyclotron frequency (11 GHz) in MST, only $\sim 1.5\%$ error occurs when using the individual probe-LO mixing products to obtain the interferometer phase shift. The individual phase of each of the mixing products is determined with respect to a reference mixer by use of a digital phase comparator technique.¹⁵

The three-wave FIR laser source is optically pumped by an infrared CO₂ laser (continuous output 140 W) and operated at 432.5 μm (694 GHz; 25 mW/cavity). The three FIR cavities will be operated such that the IF between the two slave cavities and the master cavity are 600 and 900 kHz. These frequencies will be multiplexed onto a single mixer for each chord and reference along with the beat frequency between the two slave cavities at 300 kHz. This will provide a 4 μs time response for the simultaneous polarimeter–interferometer measurement. Both the probe and local-oscillator beams are subdivided for the discrete vertically viewing ports covering most of the plasma cross section. Corner-cube GaAs Schottky-diode mixers are used as detectors in the receiver where the probe and local-oscillator beams are combined. The combined polarimeter–interferometer system (see Fig. 2) consists of 11-chords divided between toroidal azimuths 250° (five chords located at $x=R-R_0=36, 21, 6, -9,$ and -24 cm) and 255° (six chords located at $x=R-R_0=43, 28, 13, -2, -17,$ and -32 cm). Calibration of the polarimeter system, necessitated by the asymmetric reflection-transmission properties of the wire mesh beamsplitters,¹⁶ is achieved through rotation of an additional half-wave plate placed in the probe-beam path. Details of this procedure have been described elsewhere.¹⁷ Typical polarimeter system rms noise levels are 1 mrad ($\approx 0.1^\circ$) at 100 kHz bandwidth [0.4 mrad (0.04°) at 20 kHz bandwidth]. The data can be ensemble averaged over similar time windows (e.g., sawtooth cycle) for further noise reduction.

Experimental work is carried out on the Madison Symmetric Torus (MST) RFP which is ohmically heated with major radius $R_0=1.50$ m and limiter radius $a=0.51$ m. Data

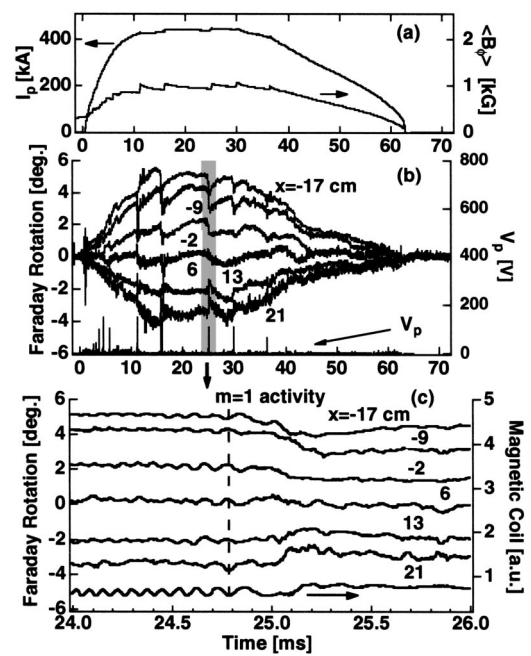


FIG. 3. (a) Plasma current and average toroidal magnetic field; (b) Faraday rotation angle for standard Ohmic MST plasma from six polarimeter chords; (c) expanded time scale. Sawtooth crashes are denoted by the prompt generation of toroidal magnetic field and spikes in poloidal voltage, V_p . Faraday rotation data are low-pass filtered with 20 kHz cutoff.

presented are for deuterium plasmas with toroidal current $I_p=400$ kA and nominal electron density $n_e=1 \times 10^{19} \text{ m}^{-3}$.

III. EXPERIMENTAL RESULTS

The first tests of the 11-chord fast POLARIS diagnostic have recently been conducted on MST. For these tests, the two available far-infrared probe beams are frequency offset at 750 kHz (1.4 μs minimum time response) and set to counter-rotating circular polarization. Without the LO beam, the simultaneous interferometry capability is lost but the full polarimetry capability can be realized. The mixer for each channel then detects the mutual mixing product of the two probe beams which is directly proportional to twice the Faraday rotation angle as described by Eq. (1). The data are sampled at 1 MHz with the difference frequency being aliased to 250 kHz.

Typical MST polarimetry data for a standard sawtooth discharge with $I_p=400$ kA, bandpass filtered at 20 kHz, are shown in Fig. 3. All chords show a strong correlation with the sawtooth cycle, even during the setup phase of the discharge (0–10 ms). Sawtooth crashes, characterized by changes in toroidal flux, are denoted by prompt increases in the average toroidal field, $\langle B_\phi \rangle$ and spikes in the surface poloidal voltage, V_p . As expected, the Faraday rotation angle changes sign about the magnetic axis due to a change in the direction of the poloidal magnetic field with respect to the polarimeter chords. Zero Faraday rotation angle indicates that the probing beam passes through the magnetic axis. The sawtooth crash represents a discrete dynamo event in the RFP.

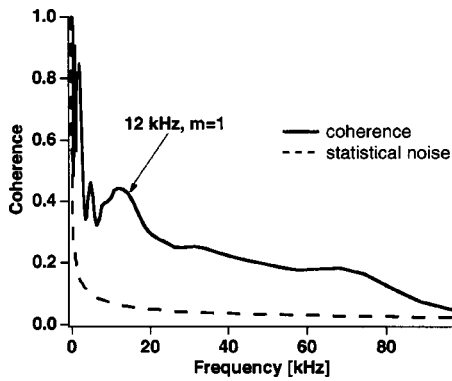


FIG. 4. Coherence between $x=21$ cm polarimeter chord and external magnetic sensing coil. Solid (dashed) line corresponds to coherence (statistical noise).

In Fig. 3(c), the time axis is expanded to isolate an individual sawtooth crash ($t=25$ ms). The typical sawtooth crash or relaxation time scale is measured to be $\approx 100\text{--}200 \mu\text{s}$. A clear coherent oscillation is observed on all chords prior to the sawtooth crash. The frequency of these fluctuations matches the dominant $m=1$ tearing mode in MST (as measured by external magnetic coils) and have frequency peaking near 12 kHz. Finite coherence is observed at frequencies up to 100 kHz when computing the coherence between a polarimeter chord and an external magnetic coil as shown in Fig. 4. This measurement demonstrates two important facts: (1) The fast polarimeter not only has sufficient time response, but also the phase resolution necessary to observe high-frequency small-amplitude fluctuations, and (2) Faraday rotation fluctuations are strongly correlated with magnetic field fluctuations in MST.

Since the polarimeter measures the line-integrated product of density and magnetic field [see Eq. (1)], changes observed in the Faraday rotation signal likely correspond to changes in both parameters. With these results, it is now possible to extract information on the plasma poloidal magnetic field, current density profile, their temporal evolution and magnetic fluctuations.

A. Equilibrium measurements

Equilibrium analysis of the Faraday rotation data can be accomplished using any one of three independent techniques, of increasing complexity, to arrive at information on the current density distribution. The simplest analysis yields the central current density from the slope of the Faraday rotation profile at the center according to the relation

$$J(0) = \frac{2}{\mu_0 c_F} \frac{d\Psi}{dx} \frac{1}{\int n_e f(r, \alpha) dz}, \quad (3)$$

where c_F is a constant and $f(r, \alpha)$ represents the current profile shape [estimated from the total current $I_p = J(0) \int 2\pi r f(r, \alpha) dr$]. This leaves us with a relation for $J(0)$ which is proportional to the slope of the Faraday rotation signal across the magnetic axis, $d\Psi/dx$. The next approach employs a fitting method to solve Eq. (1) and yields the toroidal current density profile. The most complex analysis utilizes a two-dimensional equilibrium reconstruction code (solving the Grad–Shafranov equation) to yield the cur-

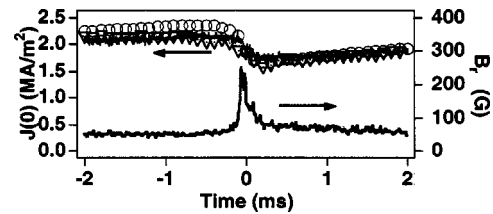


FIG. 5. Comparison of \bar{B}_r and $J(0)$ through the sawtooth cycle (crash occurs at $t=0$). $J(0)$ is determined from Eq. (3) (solid line), cylindrical equilibrium model (open circles, $\beta=7\%$), and functional fit analysis (open triangles). Ensembled data are used.

rent density as a function of magnetic surface coordinate. All three techniques provide consistent information on $J(r)$ and have been described previously.¹⁸ To obtain the necessary polarimetry and interferometry data for equilibrium analysis, the system is first operated in polarimeter mode for 20–30 similar shots and then converted to interferometer mode for a similar number of shots to obtain the electron density. The data are ensemble averaged over the sawtooth cycle producing the profile change averaged over ~ 400 sawtooth events.

Direct experimental measurement shows that the current density on axis drops by 20% during the sawtooth relaxation. Comparison of $J(0)$ estimated from the slope of the Faraday rotation angle across the magnetic axis with $J(0)$ from a simple cylindrical equilibrium model¹⁹ is shown in Fig. 5 and the two agree quite well in both absolute value and temporal history. The agreement, within measurement errors of $\sim 10\%$, bolsters confidence in both the measurement technique and the cylindrical equilibrium model. The current density decrease at the sawtooth crash can potentially be explained by the MHD dynamo which is predicted to drive antiparallel current in the plasma core.²⁰

Faraday rotation profiles, taken from the ensembled data, at times immediately before (-0.25 ms) and after ($+0.25$ ms) the sawtooth crash are shown in Figs. 6(a) and 6(b), respectively. The magnetic axis corresponds to the point where $\Psi=0$ and is shifted $\sim 4\text{--}5$ cm outward from the center of the conducting boundary. Reduced slope ($d\Psi/dx$), proportional to reduced current density on axis, is evident for the central chords after the sawtooth crash. The maximum rotation angle (absolute value) is larger on the inboard side due to the toroidicity of the plasma.

By use of the functional fitting technique, toroidal current density (J_ϕ) profiles corresponding to times before and after the sawtooth crash are generated and shown in Fig. 7(a). Corresponding fits to the measured Faraday profiles are

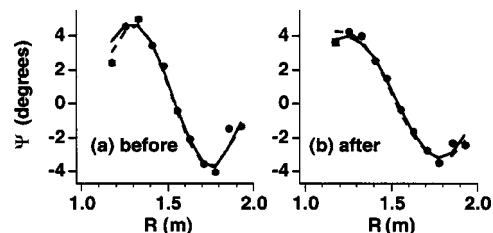


FIG. 6. Measured Faraday rotation profiles at times (a) 0.25 ms before and (b) 0.25 ms after the sawtooth crash. Symbols represent the measurement points (error bars approximately equal symbol size), solid lines the functional fit and dashed lines the MSTFIT matching.

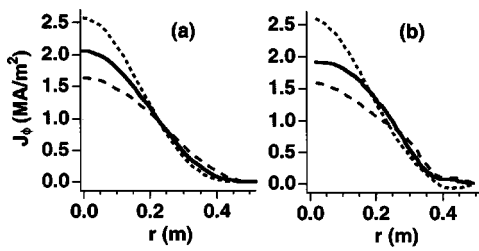


FIG. 7. Toroidal current density profile generated by (a) functional fit approach and (b) MSTFIT for times 0.25 ms before (solid), 0.25 ms after (long dash), the sawtooth crash and during PPCD (short dash).

shown as solid lines in Figs. 6(a) and 6(b). The toroidal current density indicates a clear reduction in the plasma core, $r < 0.2$ m, and increase towards the outside, $r > 0.2$ m, immediately after the sawtooth crash. The decreased interior current density is in excellent agreement with Fig. 5. After the crash, the flattened profile begins to slowly narrow and peak on axis until the next sawtooth or relaxation event. The toroidal current density is very small in the edge where the toroidal field reverses and the parallel direction is predominantly poloidal.

The toroidal current density determined from the equilibrium reconstruction code MSTFIT²¹ is shown in Fig. 7(b). Inputs to the toroidal equilibrium code include the external magnetics, pressure profiles, motional Stark effect measurements of $B(0)$, as well as the Faraday rotation data. The corresponding fits to the Faraday rotation profile [see Figs. 6(a) and 6(b)] are nearly indistinguishable from the functional fit result, and both match the measured Faraday rotation profile quite well. The current density profile is very sensitive to changes in the Faraday profile. Differences in toroidal current density shape between the functional fit and equilibrium reconstruction approaches provide an indication of errors in the resulting profiles. Both results show the same general features of a peaking current density distribution which flattens significantly at the sawtooth crash.

High-confinement plasmas are achieved in MST by inductively driving parallel current in the edge through a process called pulsed parallel current drive or PPCD. PPCD acts to suppress sawteeth and reduce the $m=0$ and $m=1$ resistive tearing modes that limit energy and particle confinement in RFP plasmas. Field reversal is maintained via external drive rather than the dynamo. For these improved-confinement plasmas, both the energy and particle confinement time are observed to increase tenfold.^{2,22} As shown in Fig. 7, from both the functional fit and MSTFIT equilibrium reconstruction, distinct peaking of the toroidal current density in the plasma core is observed during PPCD. The current density on axis increases by 30% compared to the pre-sawtooth-crash value while the current tends to decrease at the edge. This peaking may be explained by a reduction in the “dynamo effect” and the emergence of high-energy runaway electrons that accompany the fluctuation reduction.

B. Fluctuation measurements

Since the measured Faraday rotation angle depends on both the density and magnetic field, it is necessary to sepa-

rate the two in order to isolate the fluctuating magnetic field.^{3,23} By rewriting Eq. (1) in terms of the equilibrium and fluctuating quantities for each variable (e.g., $\Psi = \Psi_0 + \tilde{\Psi}$, $B_z = B_{0z} + \tilde{B}_z$, $n_e = n_0 + \tilde{n}$), the fluctuating part of the Faraday rotation signal becomes

$$\tilde{\Psi} = c_F \left(\int B_{0z} \tilde{n} dz + \int \tilde{B}_z n_0 dz \right), \quad (4)$$

where the second order term, $c_F \int \tilde{B}_z \tilde{n} dz$, is negligible because both \tilde{n} and \tilde{B}_z are small. From this equation we see that the fluctuating part of the polarimetry signal is the sum of the fluctuating electron density weighted by equilibrium magnetic field, and the fluctuating magnetic field weighted by equilibrium density.

For all polarimeter chords shown in Fig. 3(c), the $\int B_{0z} \tilde{n} dz$ term of Eq. (4) is negligible and $\tilde{\Psi} \approx c_F \int \tilde{B}_z n_0 dz$. By using measured values for equilibrium poloidal magnetic field and electron density fluctuations, it can be shown that $\int B_{0z} \tilde{n} dz < 0.04^\circ$, which is less than the polarimeter rms noise level (0.1°). Finite contributions from the toroidal magnetic field to the Faraday signal resulting from misalignment have also been considered and found to be negligible.

Phase measurements indicate that fluctuations (both density and magnetic field) with frequencies > 5 kHz have poloidal mode number $m=1$. For the central interferometer chords, we measure $\int \tilde{n} dz \rightarrow 0$ since a line-averaged measurement of an $m=1$ density perturbation cancels out along the chord.²⁴ However, for the magnetic field, an $m=1$ perturbation above and below the midplane points in the same direction along the chord thereby adding to give a maximum, consistent, with experimental observations. For the central chord (i.e., $x=6$ cm), the fluctuating Faraday rotation signal provides a chord-integrated measurement of radial magnetic field fluctuations.

The line-integrated magnetic fluctuation amplitude can be estimated from the relation $\tilde{B}_r \equiv (\bar{n}_0 \Delta z)^{-1} \int n_0 \tilde{B}_z dz \equiv (c_F \bar{n}_0 \Delta z)^{-1} \tilde{\Psi}$. Using the measured line-averaged density (\bar{n}_0), chord length (Δz) and Faraday rotation, we find the time-averaged rms amplitude of the magnetic field fluctuations, $\tilde{B}_r \sim 33$ G or $\tilde{B}_r / B_0 \sim 0.6\%$, for the data shown in Fig. 3(c). The polarimeter rms noise level is ~ 10 G. Since the density profile is centrally peaked, the line-averaged \tilde{B}_r measurement is weighted to the plasma core. In addition, output from a 3D, nonlinear, resistive MHD simulation²⁵ predicts that the eigenfunctions for the dominant tearing modes in MST (i.e., $m=1$, $n=5-10$, $f \sim 10-20$ kHz) peak in the plasma core. Both of these factors suggest that the measured \tilde{B}_r is primarily a measure of magnetic fluctuations in the plasma core.

Information on the magnetic fluctuation poloidal mode number can be obtained by measuring the phase difference between chords along the same major radius. This reveals that fluctuations with frequency < 5 kHz are $m=0$ while higher frequency fluctuations are $m=1$. The toroidal mode number (n) spectrum and dispersion relation can be determined by applying two-point correlation techniques to toroi-

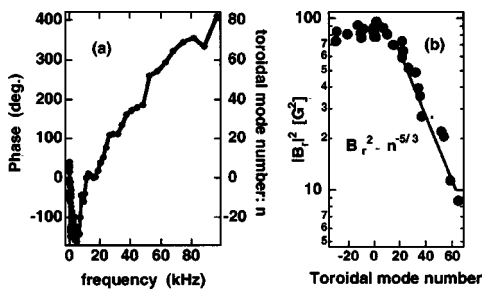


FIG. 8. Magnetic fluctuation (a) dispersion and (b) toroidal mode number spectra.

dally displaced polarimeter chords (chords at $x = -9$ and 6 cm are offset 5° toroidally from chords at $x = -2$ and 13 cm). The cross-phase between toroidally offset chords ($\Delta\phi$) can be related to toroidal wave number (k_ϕ) through the relation $k_\phi = \Delta\phi/d = n/R$, where d is the distance between the chords.¹ Magnetic fluctuation dispersion and toroidal mode number spectra for a standard sawtooth MST plasma are shown in Fig. 8. An upper bound on the measured wave number, k_ϕ , is determined by the chord width and corresponds to $\sim 1 \text{ cm}^{-1}$. Measured mode velocities are consistent with external coil measurements. The toroidal mode number spectrum, like the frequency spectrum, is broad but peaked at $|n| = 5-10$. This corresponds to the dominant core-resonant modes. Modes with $n < 0$ originate in the plasma core while modes with $n > 0$ are from outside the reversal surface ($r/a \sim 0.85$) where $q = 0$. For high n modes, the magnetic fluctuation energy spectrum falls off as $n^{-5/3}$.

Equilibrium magnetic field measurements and equilibrium reconstruction indicate that at the midplane, the $q = m/n = 1/6$ rational surface is located between chords ($x = 13$ and 21 cm) and ($x = -9$ and -17 cm). The π phase change observed on the polarimeter chords across this region [see Fig. 3(c)] is consistent with expectations for a current channel associated with the island. By applying Ampere's law to the loop between adjacent chords, one can estimate the toroidal current perturbation associated with the island. A maximum occurs when choosing chords with out-of-phase oscillations indicating the current density perturbation for the ($m/n = 1/6$) mode is approximately $\tilde{j}_{m=1, n=6} / J_0 \sim 3\%$ with spatial extent < 8 cm.²³

A strong correlation between internal magnetic field fluctuations and the current density dynamics is experimentally observed. The magnetic field fluctuation amplitude for ensembled data is $\tilde{B}_r / B_0 \sim 1\%$ (before the crash) but varies significantly during the sawtooth cycle as shown in Fig. 4(a). The magnetic fluctuation amplitude is fairly constant until $100 \mu\text{s}$ before the crash, when it jumps over fourfold within $\sim 50 \mu\text{s}$. The equilibrium current density gradually increases during the slow ramp phase of the cycle and promptly drops 20% at the sawtooth crash as shown in Fig. 4(b). The enhanced magnetic fluctuations are predicted to generate a dynamo electric field which acts to reduce toroidal current density in the core and increase poloidal current at the edge^{17,26,27} as evidenced by toroidal flux increase at the crash [see Fig. 3(a)].

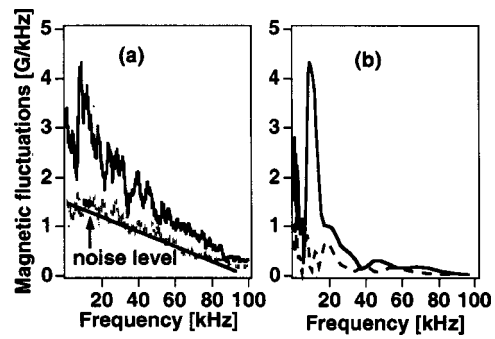


FIG. 9. (a) Radial magnetic field fluctuation spectrum, and (b) coherence weighted spectrum for standard sawtooth (solid line) and PPCD (dashed line) plasmas in MST.

The core radial magnetic field fluctuation frequency spectrum for a high-confinement PPCD plasma is shown in Fig. 9(a) along with the broadband fluctuation spectrum for a standard sawtooth discharge (using 5 ms time average). Here it is clearly seen that the magnetic field fluctuation amplitude is reduced across the entire spectrum (by at least a factor of 2 for the core modes, $f \sim 10-20$ kHz). In fact, the fluctuation spectrum measured during PPCD is essentially the same as the polarimeter noise spectrum implying that we are limited by the instrumental resolution. In an effort to extract the coherent portion of the spectrum from these data, we plot the coherence-weighted frequency spectra in Fig. 9(b). The coherence weighted spectra is the product of the fluctuation spectrum and computed coherence between the $x = 6$ cm polarimeter chord and an external magnetic coil. Here we see the coherent portion of the spectrum from $10-20$ kHz, which corresponds to the dominant core modes, is reduced fourfold during PPCD. This indicates that the core fluctuation amplitude is more strongly suppressed than at the edge. A change in the radial structure of the fluctuations is implied. The reduction of core magnetic fluctuations strongly correlates with flattening of the $J_{||}$ profile at the edge (acting to suppress the magnetic fluctuations) and increased particle and energy confinement.

Temporal evolution of the Faraday rotation frequency

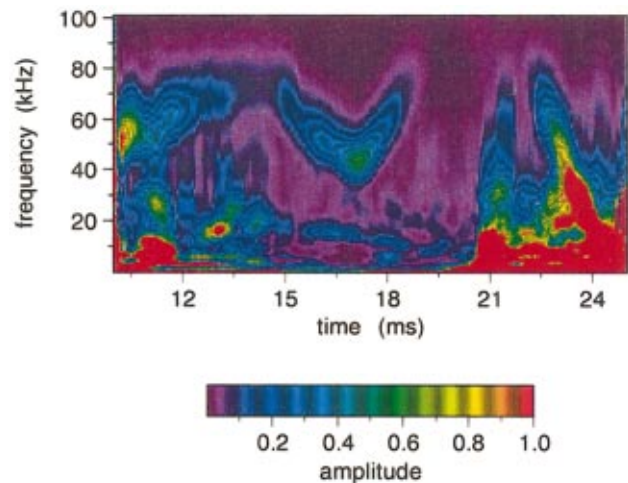


FIG. 10. (Color) Time evolution of Faraday rotation fluctuation spectrum during a quasi-single-helicity PPCD shot on MST.

spectra is shown in Fig. 10 for a PPCD discharge where the magnetic fluctuations were not completely suppressed. During the time of improved confinement (15–20 ms), a low-frequency mode (~ 10 – 20 kHz, low n) is observed to spin-up and then slow down. However, at higher frequencies (~ 40 – 80 kHz, high n) a different mode is observed to first slow down and then spin-up on the same timescale. The interplay of these various modes, which originate in different regions of the plasma, is under active investigation. This plot serves to show the dynamic nature of the magnetic fluctuations in MST and POLARIS's ability to resolve them.

IV. CONCLUSION

In summary, the poloidal magnetic field structure and magnetic field fluctuations have been nonperturbatively measured in the core of a high-temperature RFP plasma using a newly developed fast-polarimetry system, POLARIS. Future work will focus on implementing the full three-wave laser capability so that the Faraday rotation and interferometry measurements can be made simultaneously. In addition, measurements will focus on extracting the magnetic field fluctuation amplitude from all polarimeter chords in order to determine the spatial profile for the dominant global modes. Issues related to MHD stability, core-fluctuation-induced particle flux and dynamo will be addressed. The fast polarimetry technique described herein is also directly applicable to other toroidal confinement devices such as the tokamak. For a standard tokamak with $B_0 = 2$ T, the polarimeter noise level of 10 G would allow measurement of magnetic fluctuations with amplitude $\tilde{B}/B_0 \approx 5 \times 10^{-4}$.

ACKNOWLEDGMENTS

The authors wish to acknowledge and express their appreciation for the contributions of Dr. Y. Jiang, Dr. D. Holly, and Dr. N. E. Lanier. This work is supported by the U.S. Department of Energy.

¹Y. Jiang, D. L. Brower, and N. E. Lanier, *Rev. Sci. Instrum.* **70**, 703 (1999).

²N. E. Lanier, D. Craig, T. M. Biewer, B. E. Chapman, D. J. Den Hartog, C. B. Forest, S. C. Prager, D. L. Brower, and Y. Jiang, *Phys. Rev. Lett.* **85**, 2120 (2000).

³H. Soltwisch and H. R. Koslowski, *Plasma Phys. Controlled Fusion* **39**, A341 (1997).

⁴D. L. Brower, L. Zeng, and Y. Jiang, *Rev. Sci. Instrum.* **68**, 419 (1997).

⁵G. Dodel and W. Kunz, *Infrared Phys.* **18**, 773 (1978).

⁶B. W. Rice and E. B. Hooper, *Nucl. Fusion* **34**, 1 (1994).

⁷R. M. Erickson, Los Alamos National Laboratory Report LA-10731-T, June 1986.

⁸J. H. Rommers, A. J. H. Donne, F. A. Karelse, and J. Howard, *Rev. Sci. Instrum.* **68**, 1217 (1997).

⁹J. H. Rommers and J. Howard, *Plasma Phys. Controlled Fusion* **38**, 1805 (1996).

¹⁰T. Akiyama, E. Sato, T. Nozawa, S. Tsuji-Lio, R. Shimada, H. Murayama, K. Nakayama, S. Okajima, K. Tanaka, K. Watanabe, T. Tokuzawa, and K. Kawahata, *Rev. Sci. Instrum.* **72**, 1073 (2001).

¹¹T. Fukuda, S. Goto, T. Ishimura, and H. Ito, *Int. J. Infrared Millim. Waves* **5**, 1039 (1984).

¹²H. R. Koslowski, H. Soltwisch, and W. Stodiek, *Plasma Phys. Controlled Fusion* **38**, 271 (1996).

¹³V. Simic, T. P. Crowley, P. M. Schoch, A. Y. Aydemir, X. Z. Yang, K. A. Connor, R. L. Hickok, A. J. Wootton, and S. C. McCool, *Phys. Fluids B* **5**, 1576 (1993).

¹⁴X. L. Zou, L. Colas, M. Paume, J. M. Chareau, L. Laurent, P. Devynck, and D. Gresillon, *Phys. Rev. Lett.* **75**, 1090 (1995).

¹⁵Y. Jiang, D. L. Brower, L. Zeng, and J. Howard, *Rev. Sci. Instrum.* **68**, 902 (1997).

¹⁶N. E. Lanier, J. K. Anderson, C. B. Forest, D. Holly, Y. Jiang, and D. L. Brower, *Rev. Sci. Instrum.* **70**, 718 (1999).

¹⁷D. L. Brower, Y. Jiang, W. X. Ding, S. D. Terry, N. E. Lanier, J. K. Anderson, C. B. Forest, and D. Holly, *Rev. Sci. Instrum.* **72**, 1077 (2001).

¹⁸D. L. Brower, W. X. Ding, S. D. Terry, J. K. Anderson, T. M. Biewer, B. E. Chapman, D. Craig, C. B. Forest, S. C. Prager, and J. S. Sarff, *Phys. Rev. Lett.* **88**, 185005-1 (2002).

¹⁹J. S. Sarff, N. E. Lanier, S. C. Prager, and M. R. Stoneking, *Phys. Rev. Lett.* **78**, 62 (1997).

²⁰D. J. Den Hartog, J. T. Chapman, D. Craig, G. Fiksel, P. W. Fontana, S. C. Prager, and J. S. Sarff, *Phys. Plasmas* **6**, 1813 (1999).

²¹J. K. Anderson, Ph.D. dissertation, University of Wisconsin-Madison, Madison, 2001.

²²B. E. Chapman, J. K. Anderson, T. M. Biewer, D. L. Brower, S. Castillo, P. K. Chattopadhyay, C.-S. Chiang, D. Craig, D. J. Den Hartog, G. Fiksel, P. W. Fontana, C. B. Forest, S. Gerhardt, A. K. Hansen, D. Holly, Y. Jiang, N. E. Lanier, S. C. Prager, J. C. Reardon, and J. S. Sarff, *Phys. Rev. Lett.* **87**, 205001 (2001).

²³W. X. Ding, D. L. Brower, S. D. Terry, D. Craig, S. C. Prager, J. S. Sarff, and J. C. Wright, *Phys. Rev. Lett.* (submitted).

²⁴N. E. Lanier, D. Craig, J. K. Anderson, T. M. Biewer, B. E. Chapman, D. J. Den Hartog, C. B. Forest, S. C. Prager, D. L. Brower, and Y. Jiang, *Phys. Plasmas* **8**, 3402 (2001).

²⁵D. D. Schnack, D. C. Barnes, Z. Mikic, D. S. Harned, and E. J. Caramana, *J. Comput. Phys.* **70**, 330 (1987); C. R. Sovinec and S. C. Prager, *Nucl. Fusion* **39**, 777 (1999).

²⁶P. W. Fontana, D. J. Den Hartog, G. Fiksel, and S. C. Prager, *Phys. Rev. Lett.* **85**, 556 (2000).

²⁷Y. L. Ho and G. G. Craddock, *Phys. Fluids B* **3**, 721 (1991).